Analytical Methods

PAPER

# Thermophoresis of Gold Nanorods from Surface Enhanced Raman Scattering and Real-Time Rayleigh Scattering in Solution

Takuma Makihara,*[a] Steven M. E. Demers,[a] Louis E. D. Cole,[a] Aobo Zhang,[a] and Jason H. Hafner[ab]

Received 00th January 20xx,
Accepted 00th January 20xx

DOI: 10.1039/x0xx00000x

www.rsc.org/

Surface-enhanced Raman scattering (SERS) from gold and silver nanoparticles suspended in solution enables a more quantitative level of analysis relative to SERS from aggregated nanoparticles and roughened metal substrates. This is due to the more predictable and consistent near field enhancement regions created by isolated nanoparticles, and to averaging over the many nanoparticles that diffuse through the excitation beam during the measurement. However, we find that localized heating of the solution by the focused excitation leads to thermophoresis which alters the nanorod concentration in the focal volume and therefore impacts quantitative analysis. Since many phenomena may impact the Raman signal, we record both the Rayleigh and Raman scattering from gold nanoparticle solutions. This allows us to distinguish molecular processes from depletion of nanoparticles in the excitation beam. We observe that the concentration of nanorods can deplete to less than 50% of its original value over 100-second timescale, which are consistent with a thermophoretic effect driving nanoparticles from the beam spot. We also find that the particle motion drives convection within the sample cell that further contributes to signal instabilities.

## 1. Introduction

Surface-enhanced Raman scattering (SERS) provides vibrational spectra of trace quantities of chemicals near resonantly excited plasmonic structures or on rough metal surfaces. While the detailed nature of the enhancement depends on many factors, it is primarily driven by the enhanced electromagnetic near field of the nanostructure, which acts as a near-field lens to focus the incident light, and as an antenna to amplify the scattered light. [1-3] A major focus of research on SERS has been on the fabrication of plasmonic substrates that provide large enhancement, good uniformity, and low production cost. [4-9] Such substrates typically feature a high density of sharp tips and/or electromagnetic "hot spots" that occur in gaps between nanostructures. SERS substrates have been fabricated by surface texturing, random colloidal aggregation, controlled nanoparticle self-assembly, and various forms of nanoscale lithography.

Alternatively, SERS can be recorded from isolated nanoparticles suspended in solution. Although not as widely pursued as substrates, solution-phase SERS provides more reproducible measurements, albeit with lower enhancement and weaker signals. This approach has enabled studies of the nature of molecular adsorption on nanoparticle surfaces, [10-12] nanoparticle assembly and aggregation, [13-19] SERS enhancement mechanisms, [20] the limits of sensitivity, [21, 22] and the molecular structure at the nanoparticle surface. [23]

The stability in time of substrate and solution-phase SERS signals is essential when tracking changes in peak intensity. Many effects lead to temporal changes in SERS signal, including: (1) molecular processes such as desorption from the nanosurface causing signal decay, [24-29] (2) optical forces trapping nanoparticles or creating aggregation-induced hot spots causing signal increase, [30-32] or (3) thermal motion decreasing the number of hot spots and causing signal decay [33].

Many studies rely exclusively on Raman spectra when studying the instability of SERS signal. However, Raman spectra cannot always isolate the cause of signal instabilities from the three aforementioned effects. Here, we combine Raman and real-time Rayleigh scattering measurements from isolated nanoparticles in solution to isolate molecular effects from optical or thermal effects. Using a model based on thermophoresis, we conclude that our observed SERS signal instability is thermal in nature. [34-37] We also present evidence for convection in solutions subjected to prolonged laser irradiation. Understanding the nature of variation in solution-phase SERS signals will aid future studies that use this powerful spectroscopic approach.

[a] Department of Physics & Astronomy, Rice University, Houston, Texas, 77251, United States
[b] Department of Chemistry, Rice University, Houston, Texas, 77251, United States

Electronic Supplementary Information (ESI) available: Fig. S1 Extinction spectrum of gold nanorods. Fig. S2 Lack of hysteresis in SERS signal versus excitation power. A calculation of the timescale for particle motion due to radiation pressure. Fig. S3 Comparison of Rayleigh scattering both on and off the plasmon resonance.

## 2. Methods

Gold nanorods suspended in cetyltrimethylammonium bromide (CTAB) with a nominal diameter of 50 nm and lengths of 150 - 160 nm were purchased from Nanopartz. The nanorods arrived with a nominal peak plasmon resonant absorbance of 1 for a 1 cm path and a nanoparticle concentration of $10^{10}$ nanorods/mL based on a calculated extinction cross section. The extinction spectrum of the gold nanorods are provided in Figure S1 of the Supporting Information.

Chloroform solutions of 1,2-dioleoyl-*sn*-glycero-3-phosphocholine (DOPC) and 1,2-dioleoyl-*sn*-glycero-3-phospho-(1'-*rac*-glycerol) (DOPG) were purchased from Avanti Polar Lipids. Solutions of small unilamellar lipid vesicles (SUV) were prepared by combining DOPC and DOPG in a 9:1 molar ratio and evaporating the chloroform under inert nitrogen gas. The lipid film was then rehydrated with DI water to form multilamellar vesicles at 10 mg/mL, then water bath sonicated until the solution was clear, indicating the transformation from large multilamellar vesicles to small unilamellar vesicles.

1 mL of CTAB-stabilized nanorod solution was sedimented by centrifugation at 4500 rpm for 15 min, and the clear CTAB solution was discarded. For CTAB SERS measurements, nanorods were resuspended in 1 mL of 10 mM CTAB. This was repeated three times to ensure the nanorods were suspended in a known concentration of CTAB. For lipid SERS measurements, the nanorods were resuspended in 0.2 mL of phospholipid SUV prepared as described above. This was repeated three times to ensure the nanorods were suspended in phospholipids. Zeta potential measurements before and after lipid exposure were carried out with a Zetasizer Nano (Malvern). The decrease in zeta potential from 36.5 mV for CTAB-supported nanorods to -50.7 mV for DOPC/DOPG supported nanorods is due to the anionic DOPG lipid and indicates successful ligand exchange. To increase Raman scattering signal, nanorod samples were concentrated to have a plasmon resonant absorbance of 7 after the final sedimentation. The LSPR spectral extinction peak was measured to confirm the plasmon resonant absorbance and to confirm the nanorods did not aggregate during sedimentation, which would be apparent by a red-shift in the resonant extinction peak.

For SERS experiments, nanorods suspended in CTAB or phospholipid SUV were collected in a rectangular glass capillary that had dimensions of 0.10 x 2.00 mm (VitroCom, 5012). The glass capillary was held with the 0.10 mm wide windows parallel to the table. The SERS excitation source was an 80 mW, 785 nm diode laser (Ondax) which was passed through a variable neutral density filter to lower the power at the sample and was incident on the glass capillary at the center of the 2.00 mm wide window. A 40x/0.5 N.A. near-infrared objective focused the excitation 50 μm past the window into the nanorod suspension and collected the scattered light, which passed through a dichroic mirror, through a notch filter, was dispersed with an Acton SpectraPro150, and was detected with a Princeton Instruments PIXIS CCD. Because the excitation beam was focused only 50 μm into the solution, the intensity lost due to absorption is negligible. With the nanorods freely diffusing in solution, SERS measurements were averaged over nanoparticles as they diffused through the beam over the exposure period. SERS measurements were taken using 5 minute exposure times and at increasing power from 5 mW up to 20 mW, measured at the sample, by adjusting a variable neutral density filter. The peak wavelength data were found by fitting Gaussian peaks to the plasmon resonant extinction peak and calculating the integrated area. Error bars were calculated based on the CCD counts under the peak before normalizing by integration time, excitation power, or nanorod LSPR absorbance. The error bars, which are on the order of 1% of measured values, are quite small given that a typical peak has on the order of $10^4$ counts. In the case of CTAB, the strength of Raman scattering signal was measured by tracking the strength of the bands at 760 $cm^{-1}$ and 1450 $cm^{-1}$, which correspond to the symmetric stretch of the trimethylammonium head group and twist and wag vibrations of the $CH_2$ groups, respectively. In the case of DOPC, the strength of the Raman scattering signal

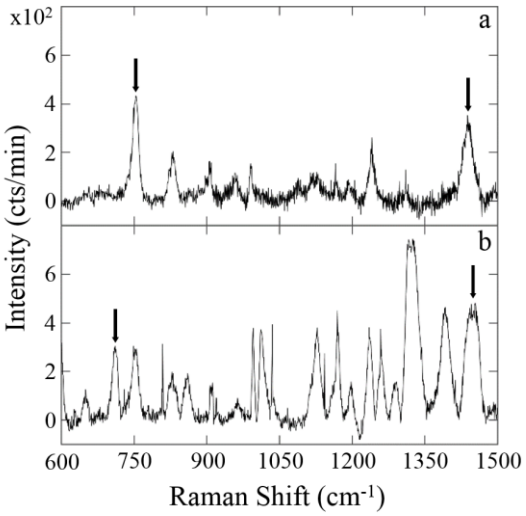


**Figure 1** SERS spectra from suspensions of $10^{10}$ gold nanorod/mL suspended in (a) 10 mM CTAB and (b) 15 mM DOPC.

was measured by tracking how the band at 718 $cm^{-1}$, which corresponds to the symmetric stretch of the choline head group, and the band at 1450 $cm^{-1}$, which corresponds to the $CH_2$ twist and wag vibrations.

Rayleigh scattering measurements were taken with the same experimental setup as the SERS measurements, but with a neutral density filter replacing the notch filter. The intensity of the scattered light was measured in real time by selecting a 4x4 pixel region of interest that contains the image of the scattered light from the focussed beam.

## 3. Results and discussion

The CTAB surfactant interacts strongly with gold nanorods via the bromide ion bound to the gold surface, and is critical to nanorod synthesis and colloidal stability.[38] CTAB is thought to form a bilayer on the nanorod surface, based on thermogravimetric analysis, transmission electron microscopy, and small angle x-ray and neutron scattering.[39, 40] A structural analysis using SERS measurements and theoretical calculations of both the electromagnetic near field and the Raman tensor found the bilayer of a similar surfactant to be tilted 27 degrees from the normal.[23] Phosphocholine lipids, which terminate in a similar chemical structure to CTAB, displace the surfactant to form a lipid bilayer on the nanorod surface. [12, 41-46] The SERS spectra of both CTAB surfactant and DOPC lipid on gold nanorods are presented in Figure 1. The best spectral feature to distinguish the two molecules is the symmetric stretch of the trimethylammonium headgroup which is found at 760 $cm^{-1}$ for CTAB and 718 $cm^{-1}$ for phosphatidylcholines.

To compare the results of different SERS experiments, we normalize the signal counts by the excitation power, integration time, and nanorod LSPR absorbance as suggested above, and therefore plot the signal in units of counts/min-mW-OD. Here OD refers to the plasmonic peak spectral absorption through a 1 cm path length, which is proportional to the nanorod concentration. Figure 2 displays the 760 $cm^{-1}$ symmetric headgroup stretch of CTAB as a function of excitation power. While one would expect the normalized signal to be constant, it decays with increasing excitation power. When the power is lowered to its original value, the signal returns to the original value with no hysteresis (see Supporting Information Figure S2).

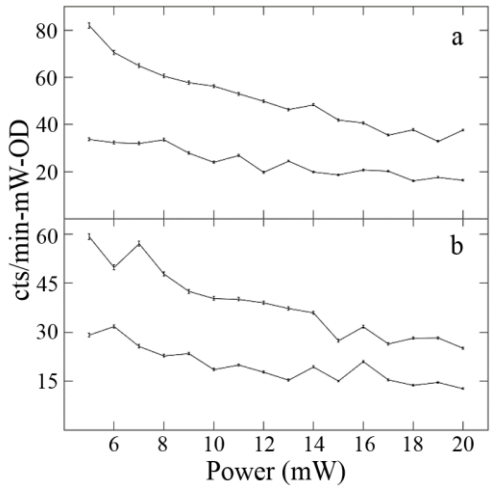


**Figure 2** The SERS intensity with increasing excitation power for (a) two modes of CTAB and (b) two modes of DOPC. In each case the 1450 $cm^{-1}$ $CH_2$ scissor mode is the top plot and the 718/760 $cm^{-1}$ symmetric headgroup stretch is the lower plot. Error bars were calculated as described above. Excitation power was measured at the sample.

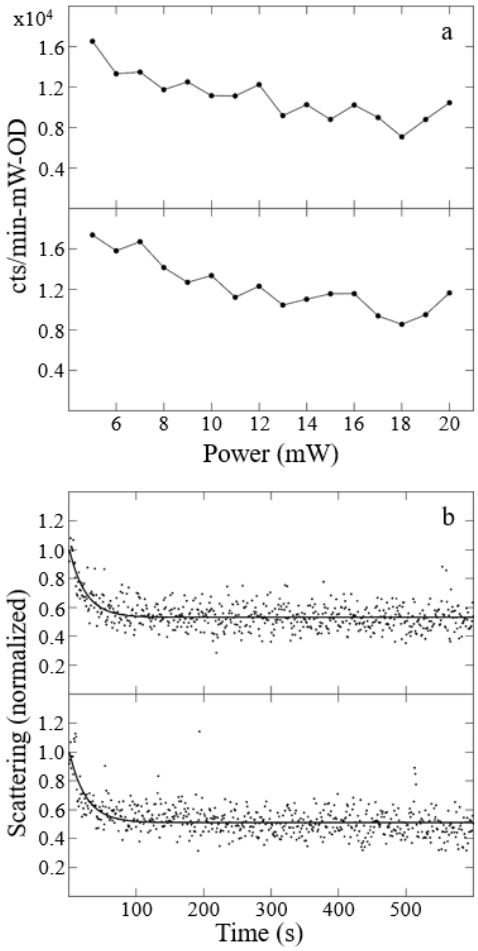


**Figure 3** The effect of the excitation beam on Rayleigh scattering. (a) The steady-state intensity at increasing excitation powers for CTAB (top) and DOPC (bottom). (b) The real-time signal decay for 20 mW excitation power for CTAB (top) and DOPC (bottom).

A possible cause is optical forces on nanoparticles, although they typically trap and concentrate the nanorods, so would increase the SERS signal rather than decrease it. Furthermore, our optical intensity is not at the level usually needed to trap or otherwise manipulate gold nanoparticles in this size range.[47-52] Radiation pressure deflecting nanorods out of the focal volume was also considered, as recent work has found radiation pressure has a non-trivial impact on solution-phase SERS experiments.[30] However, the time taken for nanorods to be forced out of the focal volume under radiation pressure was calculated to be on the order of $10^{-2}$ seconds (see Supporting Information) and is inconsistent with the timescale of signal decay measured here (Figure 3b). Another possibility is that heating by the laser beam desorbs molecules from the nanorod surface to reduce SERS signals. However, the effect appears to be universal when comparing different vibrational modes within a molecule and different molecules. Figure 2a displays the effect for CTAB modes of both the headgroup and alkane

chain. Uncorrelated fluctuations between the vibrational modes are due to concentration variations possibly from convection or optical variations from removing the sample between measurements to adjust excitation power at the sample. If elevated temperatures were causing some molecular rearrangement, the two signals would likely not decrease together, but rather exhibit sudden changes as seen previously for structural transitions of the surfactant layer.[11] One would also expect molecular desorption to vary for different molecules, but Figure 2b displays a similar result for two vibrational modes of DOPC. The similar trend in all four plots in Figure 2 suggests that the effect is universal and not dependent on a specific molecular interaction.

The signal decrease displayed in Figure 2 may simply be due to a reduction in the number of nanorods in the beam spot, rather than a molecular mechanism. Rayleigh scattering from the nanorods is a better probe of this effect since it is unaffected by surface chemistry. Also, Rayleigh scattering is a much stronger signal and therefore can be observed on a faster timescale. Figure 3a displays the normalized intensity of the Rayleigh scattered 785 nm excitation light. The Rayleigh scattering signal decreases in a manner similar to the SERS signals in Figure 2 and furthers the argument that the reduction in SERS signal is independent of surfactant/lipid desorption and is caused by nanorods being displaced from the focal volume.

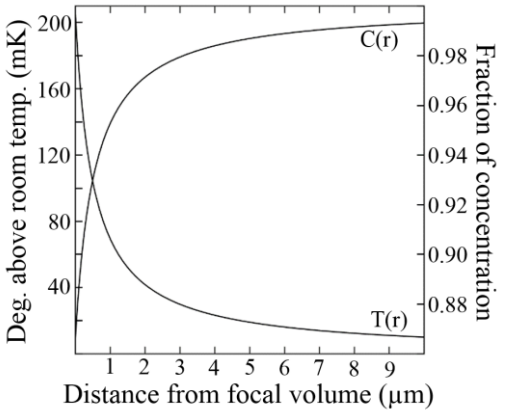


**Figure 4** The calculated temperature and concentration gradients in solution for suspensions of $10^{10}$ gold nanorod/mL under 10 mW excitation

To probe the nature of the nanoparticle displacement from the beam spot, the time dependence of the Rayleigh scattering was measured. Figure 3b shows the real-time decay of the Rayleigh scattering for CTAB and lipid supported gold nanorods fitted to exponential decays. The time constant for CTAB is 24.2 (with 95% confidence intervals of 20.2 to 30.1) and for DOPC is 24.7 (with 95% confidence intervals of 20.4 and 31.3). They decay to a steady state value on a 100 second timescale, which suggests a diffusion related mechanism.[53, 54] With increasing excitation power, the steady state value decreases. In fact, Figure 3a is taken from the steady state value of many real-time plots like those of Figure 3b. Control experiments on the Rayleigh scattering from lipid vesicles without nanorods were recorded and no signal decay was found.

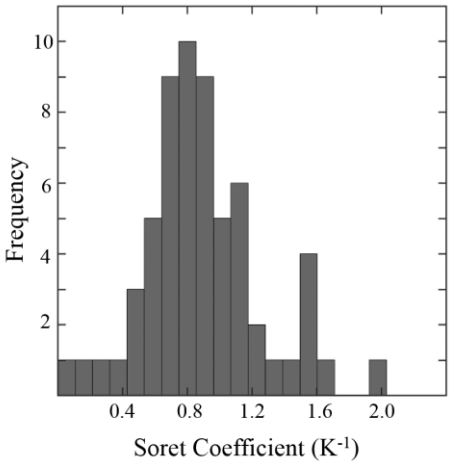


**Figure 5** A histogram of measured Soret coefficients.

It is possible that the laser-induced nanoparticle depletion observed is caused by localized heating in the nanoparticle solution. This effect is referred to as thermophoresis, or thermodiffusion for particles approaching the size of the solvent molecules,[55] and is a phenomenon whereby particles are displaced by a temperature gradient. The thermodiffusion coefficient describes diffusion away from the higher temperatures, while normal diffusion counteracts this process, resulting in a non-uniform steady state distribution. The phenomenon has been applied to proteins,[56] DNA molecules,[34] virus molecules,[57] and other colloidal solutions.[35-37] It is used as an analytical method in biochemistry to study molecular interactions.[56, 58, 59] The competing concentration and temperature gradients in the steady state are characterized by the Soret coefficient, which is defined as the ratio of the thermodiffusion coefficient to the ordinary diffusion coefficient. [34] The dependence or independence of the Soret coefficient on experimental conditions, including solvent, particle size, particle concentration, and temperature, has been studied for colloidal solutions that are similar to the gold nanorod solution used here [34-37, 60].

A simple model was developed to determine if our observations are consistent with thermophoresis. We treat the focussed laser beam as a spherical source of heat (due to nanoparticle absorption) with $r_0$ = 0.5 μm, and we assume the walls of the vitro tube are at room temperature and far away. We then solve the heat diffusion equation in spherical coordinates, which gives the temperature profile:

$$T(r) = \frac{qr_0^2}{k}\frac{1}{r} + T_0 \qquad (1)$$

where $q$ is the power absorbed by the nanorod solution, $k$ is the thermal conductivity of the medium, and $T_0$ is room temperature. The temperature increase drops as $1/r$, thus creating the thermal gradient that drives thermophoresis. At steady state, the particle flux out of the beam spot due to the temperature gradient balances the particle flux back into the beam spot driven by normal diffusion. For spherical symmetry:

$$cD_T\frac{dT}{dr} + D_c\frac{dc}{dr} = 0$$

where $c$ is the concentration, $D_T$ is the thermodiffusion constant, and $Dc$ is the normal diffusion constant. The ratio $S_T = D_T/D_c$ is called the Soret coefficient.[61] Solving for the concentration gradient and using a temperature gradient calculated from equation (1), we find an expression for the spatial variation in concentration:

$$\frac{dc}{dr} = \mathrm{c}\frac{S_T q r_0^2}{kr^2}$$

Solving this equation for the concentration profile, taking $c_0$ as the concentration far from the beam spot we find:

$$c = c_0 e^{\frac{-S_T q r_0^2}{kr}} \qquad (2)$$

for $r > r_0$.

To find quantitative estimates for the temperature increase and resulting concentration decrease near the focussed beam, the absorbed power must be estimated. Effective medium theory was used with the absorption coefficient of water (2.0 $m^{-1}$) and gold (7.7 x $10^7$ $m^{-1}$) at $\lambda$ = 785 nm radiation.[62-64] For the nanorod concentration used in the experiments the fractional gold volume was $10^{-6}$, leading to an absorption coefficient of 78.6 $m^{-1}$. For a 10 mW laser beam, the resulting power lost to absorption is 79 μW, which is converted to the heat flux $q$ using the surface area of the $r$ = 0.5 μm focal spot. Plots for the resulting temperature and concentration profiles are provided in Figure 4. The temperature increase is only on the millikelvin scale. Note that this represents the average temperature of the solution since effective medium parameters were assumed. The temperature increase at the nanorod surface will be higher. Surface temperature measurements based on Brownian fluctuations indicate a temperature increase of approximately 20 K for similar experimental conditions.[65] Although the temperature increase estimated here is very small, the gradient is significant since the temperature changes over such a short distance (due to the highly localized heat source). The predicted decrease in nanorod concentration in the beam spot is about 10%, which is similar to the 25% decays seen in Figures 2 and 3 for 10 mW excitation, and reasonable considering such an approximate model. Using Equation 2 and our values for $q$, $r_0$, and $k$, we can relate the ratio of initial to steady-state concentration of nanorods in the focal volume to the Soret coefficient. In Figure 5, we display a histogram of the Soret coefficients that have been calculated from our Rayleigh scattering experiments. Based on the histogram, the Soret coefficient is 0.894 +/- 0.183. We find that this observed value for the Soret coefficient is consistent with other results for similar size colloids. [34-37]

To investigate the contribution of resonant absorption to thermophoresis, real-time Rayleigh scattering experiments (as in Figure 3b) were repeated using a 641 nm excitation source. Rayleigh scattering from on-resonance excitation (785 nm) decayed by a factor of 1.7 more than off-resonance excitation (641 nm) at identical powers (see Supporting Information Figure S3). Although 641 nm is off the plasmon resonance, optical absorption still occurs (see Supporting Information Figure S1) and thus, one expects localized heating due to off-resonance excitation. Therefore, the observation of a smaller magnitude decay in Rayleigh scattering off-resonance is consistent with thermophoresis.

The results presented here are reproducible at the given conditions and over the ca. 500 s timescale as plotted in Figure 3b. However, we find that over longer times the SERS and Rayleigh signals tend to drift up and down in unexpected ways. We also observe spatial variations in the nanorod density for capillaries that have been exposed to the laser beam for several hours. We believe that thermophoretic forces are driving convective flows of nanorods in the thin capillaries to create these effects. An image of a capillary taken using a DSLR camera that has been exposed to an excitation beam of 785 nm and 80 mW for several hours to exaggerate the effect is displayed in

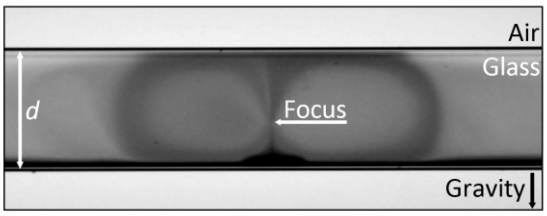


**Figure 6** A photograph of a glass capillary in which gold nanorods have been driven into motion by thermophoresis resulting in a convection pattern. The laser beam is centered on the $d$ = 2.00 mm wide window and is directed into the page.

Figure 6. Note that the capillary is 2 mm tall, so the beam focus is just a point at this scale. The settling of nanorods at the bottom of the capillary is apparent, as well as the convective flow patterns. Thermophoresis and convection have been found in the past to generate similar patterns in DNA and have been used to pattern gold nanorods on surfaces.[66, 67] Here Figure 6 provides a macroscopic visualization of the thermophoretic effects that can interfere with SERS experiments.

## 4. Conclusions

By combining Raman scattering and real-time Rayleigh scattering measurements, we have shown that thermophoresis

depletes nanoparticles in the scattering volume for typical solution-phase SERS experiments to less than 50% of its original concentration over 100 second timescales. This explains the lower relative SERS signal at higher excitation laser powers. Given our results, it is desirable to correlate SERS and Rayleigh scattering measurements in real-time and thus, we propose using a photodiode to measure real-time Rayleigh scattering during SERS experiments.

Our findings reveal that comparing experimental results and calculating surface enhancement factors require an understanding of the steady-state concentration of nanoparticles, which we have shown can be characterized using Rayleigh scattering. Thermophoresis can also drive convective flow, which will result in less predictable motions of the nanorods. Understanding and addressing signal instabilities in solution-phase SERS experiments is important when using this spectroscopic technique for analytical studies in nanoscale sensing and characterization.

## Conflicts of interest

There are no conflicts to declare.

## Acknowledgements

The authors acknowledge the Welch Foundation (grant C-1761) and National Science Foundation (award number 1709084) for supporting this research.

## Notes and references

1. G. C. Schatz, M. A. Young and R. P. Van Duyne, *Surface-Enhanced Raman Scattering: Physics and Applications*, 2006, **103**, 19-45.
2. J. A. Schuller, E. S. Barnard, W. S. Cai, Y. C. Jun, J. S. White and M. L. Brongersma, *Nat Mater*, 2010, **9**.
3. M. Moskovits, *J Raman Spectrosc*, 2005, **36**, 485-496.
4. M. K. Fan, G. F. S. Andrade and A. G. Brolo, *Anal. Chim. Acta*, 2011, **693**, 7-25.
5. M. J. Banholzer, J. E. Millstone, L. D. Qin and C. A. Mirkin, *Chem Soc Rev*, 2008, **37**, 885-897.
6. P. L. Stiles, J. A. Dieringer, N. C. Shah and R. R. Van Duyne, *Annu Rev Anal Chem*, 2008, **1**, 601-626.
7. R. S. Golightly, W. E. Doering and M. J. Natan, *Acs Nano*, 2009, **3**, 2859-2869.
8. R. Gillibert, J. Q. Huang, Y. Zhang, W. L. Fu and M. L. de la Chapelle, *Trac-Trend Anal Chem*, 2018, **105**, 166-172.
9. R. Gillibert, J. Q. Huang, Y. Zhang, W. L. Fu and M. L. de la Chapelle, *Trac-Trend Anal Chem*, 2018, **105**, 185-190.
10. B. L. Darby and E. C. Le Ru, *J Am Chem Soc*, 2014, **136**, 10965-10973.
11. S. Lee, L. J. E. Anderson, C. M. Payne and J. H. Hafner, *Langmuir*, 2011, **27**, 14748-14756.
12. J. R. Matthews, C. M. Payne and J. H. Hafner, *Langmuir*, 2015, **31**, 9893-9900.
13. I. Haidar, G. Levi, L. Mouton, J. Aubard, J. Grand, S. Lau-Truong, D. R. Neuville, N. Felidj and L. Boubekeur-Lecaque, *Phys Chem Chem Phys*, 2016, **18**, 32272-32280.
14. T. A. Laurence, G. Braun, C. Talley, A. Schwartzberg, M. Moskovits, N. Reich and T. Huser, *J Am Chem Soc*, 2009, **131**, 162-169.
15. M. Meyer, E. C. Le Ru and P. G. Etchegoin, *J Phys Chem B*, 2006, **110**, 6040-6047.
16. M. M. Al-Shalalfeh, T. A. Saleh and A. A. Al-Saadi, *Rsc Adv*, 2016, **6**, 75282-75292.
17. T. A. Saleh and A. A. Al-Saadi, *Surf Interface Anal*, 2015, **47**, 785-792.
18. T. A. Saleh, M. M. Al-Shalalfeh and A. A. Al-Saadi, *Sensor Actuat B-Chem*, 2018, **254**, 1110-1117.
19. T. A. Saleh, M. M. Al-Shalalfeh, A. T. Onawole and A. A. Al-Saadi, *Vib Spectrosc*, 2017, **90**, 96-103.
20. E. C. Le Ru, M. Meyer, E. Blackie and P. G. Etchegoin, *J Raman Spectrosc*, 2008, **39**, 1127-1134.
21. E. C. Le Ru, J. Grand, I. Sow, W. R. C. Somerville, P. G. Etchegoin, M. Treguer-Delapierre, G. Charron, N. Felidj, G. Levi and J. Aubard, *Nano Lett*, 2011, **11**, 5013-5019.
22. E. C. Le Ru, M. Meyer and P. G. Etchegoin, *J Phys Chem B*, 2006, **110**, 1944-1948.
23. J. R. Matthews, C. R. Shirazinejad, G. A. Isakson, S. M. E. Demers and J. H. Hafner, *Nano Lett*, 2017, **17**, 2172-2177.
24. Y. S. Choi, J. J. Kim and S. Miyajima, *Chem Phys Lett*, 1996, **255**, 45-48.
25. M. A. De Jesus, K. S. Giesfeldt and M. J. Sepaniak, *Appl Spectrosc*, 2003, **57**, 428-438.
26. J. H. Kim, K. M. Twaddle, L. M. Cermak, W. Jang, J. Yun and H. Byun, *Colloid Surface A*, 2016, **498**, 20-29.
27. A. Weiss and G. Haran, *J Phys Chem B*, 2001, **105**, 12348-12354.
28. K. Haruna, T. A. Saleh, M. K. Hossain and A. A. Al-Saadi, *Chem Eng J*, 2016, **304**, 141-148.

 

29. K. Haruna, T. A. Saleh, J. Al Thagfi and A. A. Al-Saadi, *J Mol Struct*, 2016, **1121**, 7-15.
30. B. Fazio, C. D'Andrea, A. Foti, E. Messina, A. Irrera, M. G. Donato, V. Villari, N. Micali, O. M. Marago and P. G. Gucciardi, *Sci Rep-Uk*, 2016, **6**.
31. F. Svedberg and M. Kall, *Faraday Discuss*, 2006, **132**, 35-44.
32. Y. F. Yuan, Y. N. Lin, B. B. Gu, N. Panwar, S. C. Tjin, J. Song, J. L. Qu and K. T. Yong, *Coordin Chem Rev*, 2017, **339**, 138-152.
33. K. W. Kho, Z. X. Shen, Z. Lei, F. Watt, K. C. Soo and M. Olivo, *Anal Chem*, 2007, **79**, 8870-8882.
34. S. Duhr and D. Braun, *P Natl Acad Sci USA*, 2006, **103**, 19678-19682.
35. M. Braibanti, D. Vigolo and R. Piazza, *Phys Rev Lett*, 2008, **100**, 4.
36. R. Piazza and A. Parola, *J. Phys.-Condes. Matter*, 2008, **20**, 18.
37. Y. G. Zhao, C. L. Zhao, J. H. He, Y. Zhou and C. Yang, *Soft Matter*, 2013, **9**, 7726-7734.
38. S. E. Lohse and C. J. Murphy, *Chem Mater*, 2013, **25**, 1250-1261.
39. B. Nikoobakht and M. A. El-Sayed, *Langmuir*, 2001, **17**, 6368-6374.
40. S. Gomez-Grana, F. Hubert, F. Testard, A. Guerrero-Martinez, I. Grillo, L. M. Liz-Marzan and O. Spalla, *Langmuir*, 2012, **28**, 1453-1459.
41. J. A. Yang and C. J. Murphy, *Langmuir*, 2012, **28**, 5404-5416.
42. C. S. Levin, J. Kundu, B. G. Janesko, G. E. Scuseria, R. M. Raphael and N. J. Halas, *J Phys Chem B*, 2008, **112**, 14168-14175.
43. E. T. Castellana, R. C. Gamez and D. H. Russell, *J Am Chem Soc*, 2011, **133**, 4182-4185.
44. J. Weingart, P. Vabbilisetty and X. L. Sun, *Adv Colloid Interfac*, 2013, **197**, 68-84.
45. H. Takahashi, Y. Niidome, T. Niidome, K. Kaneko, H. Kawasaki and S. Yamada, *Langmuir*, 2006, **22**, 2-5.
46. C. J. Orendorff, T. M. Alam, D. Y. Sasaki, B. C. Bunker and J. A. Voigt, *Acs Nano*, 2009, **3**, 971-983.
47. Z. M. Li, W. Z. Mao, M. S. Devadas and G. V. Hartland, *Nano Lett*, 2015, **15**, 7731-7735.
48. P. V. Ruijgrok, N. R. Verhart, P. Zijlstra, A. L. Tchebotareva and M. Orrit, *Phys Rev Lett*, 2011, **107**, 4.
49. J. Trojek, L. Chvatal and P. Zemanek, *J. Opt. Soc. Am. A-Opt. Image Sci. Vis.*, 2012, **29**, 1224-1236.
50. C. Selhuber-Unkel, I. Zins, O. Schubert, C. Sonnichsen and L. B. Oddershede, *Nano Lett*, 2008, **8**, 2998-3003.
51. O. Brzobohaty, M. Siler, J. Trojek, L. Chvatal, V. Karasek, A. Patak, Z. Pokorna, F. Mika and P. Zemanek, *Sci Rep-Uk*, 2015, **5**, 9.
52. P. V. Ruijgrok, P. Zijlstra, A. L. Tchebotareva and M. Orrit, *Nano Lett*, 2012, **12**, 1063-1069.
53. P. Reineck, C. J. Wienken and D. Braun, *Electrophoresis*, 2010, **31**, 279-286.
54. M. Jerabek-Willemsen, T. Andre, R. Wanner, H. M. Roth, S. Duhr, P. Baaske and D. Breitsprecher, *J Mol Struct*, 2014, **1077**, 101-113.
55. M. Eslamian and M. Z. Saghir, *Int. J. Therm. Sci.*, 2014, **80**, 58-64.
56. C. J. Wienken, P. Baaske, U. Rothbauer, D. Braun and S. Duhr, *Nat Commun*, 2010, **1**, 7.
57. Z. L. Wang, H. Kriegs, J. Buitenhuis, J. K. G. Dhont and S. Wiegand, *Soft Matter*, 2013, **9**, 8697-8704.
58. S. A. I. Seidel, P. M. Dijkman, W. A. Lea, G. van den Bogaart, M. Jerabek-Willemsen, A. Lazic, J. S. Joseph, P. Srinivasan, P. Baaske, A. Simeonov, I. Katritch, F. A. Melo, J. E. Ladbury, G. Schreiber, A. Watts, D. Braun and S. Duhr, *Methods*, 2013, **59**, 301-315.
59. M. Jerabek-Willemsen, C. J. Wienken, D. Braun, P. Baaske and S. Duhr, *Assay Drug Dev Techn*, 2011, **9**, 342-353.
60. D. Lusebrink and M. Ripoll, *J Chem Phys*, 2012, **137**, 11.
61. S. A. Putnam and D. G. Cahill, *Langmuir*, 2005, **21**, 5317-5323.
62. J. A. Curcio and C. C. Petty, *J Opt Soc Am*, 1951, **41**, 302-304.
63. P. B. Johnson and R. W. Christy, *Phys Rev B*, 1972, **6**, 4370-4379.
64. W. S. Pegau, D. Gray and J. R. V. Zaneveld, *Appl Optics*, 1997, **36**, 6035-6046.
65. F. Hajizadeh, L. Shao, D. Andren, P. Johansson, H. Rubinsztein-Dunlop and M. Kall, *Optica*, 2017, **4**, 746-751.
66. D. Braun and A. Libchaber, *Phys Rev Lett*, 2002, **89**.
67. H. T. Chen, E. Gratton and M. A. Digman, *Biophys J*, 2016, **110**, 505a-506a.